



Research paper

Structure-based discovery of selective BRPF1 bromodomain inhibitors

Jian Zhu ^a, Chunxian Zhou ^b, Amedeo Caflich ^{a,*}^a Department of Biochemistry, University of Zurich, Winterthurerstrasse 190, CH-8057, Zurich, Switzerland^b Department of Pathology, Shanghai University of Traditional Chinese Medicine, Cailun Road 1200, Pudong District, Shanghai, China

ARTICLE INFO

Article history:

Received 15 December 2017

Received in revised form

5 April 2018

Accepted 23 May 2018

Available online 2 June 2018

Keywords:

BRPF1 bromodomain

Pharmacophore search

Structure-based drug design

X-ray crystallography

Isothermal titration calorimetry

Molecular dynamics

ABSTRACT

Bromodomain and plant homeodomain (PHD) finger containing protein 1 (BRPF1) is a member of subfamily IV of the human bromodomains. Experimental evidence suggests that BRPF1 is involved in leukemia. In a previous high-throughput docking campaign we identified several chemotypes targeting the BRPF1 bromodomain. Here, pharmacophore searches using the binding modes of two of these chemotypes resulted in two new series of ligands of the BRPF1 bromodomain. The 2,3-dioxo-quinoline **21** exhibits a 2- μ M affinity for the BRPF1 bromodomain in two different competition binding assays, and more than 100-fold selectivity for BRPF1 against other members of subfamily IV and representatives of other subfamilies. Cellular activity is confirmed by a viability assay in a leukemia cell line. Isothermal titration calorimetry measurements reveal enthalpy-driven binding for compounds **21**, **26** ($K_D = 3 \mu\text{M}$), and the 2,4-dimethyl-oxazole derivative **42** ($K_D = 10 \mu\text{M}$). Multiple molecular dynamics simulations and a dozen co-crystal structures at high resolution provide useful information for further optimization of affinity for the BRPF1 bromodomain.

© 2018 Elsevier Masson SAS. All rights reserved.

1. Introduction

Bromodomains are evolutionarily conserved protein-protein interaction modules that selectively bind to acetyl-lysine (Kac) residues. They recognize acetylated histone tails, and are thus involved in the regulation of gene expression. Human proteome analysis indicates that there are eight bromodomain subfamilies, with 61 members found in 42 diverse proteins. Bromodomain-containing proteins have important role in biological process and are functionally implicated in disease processes, including cancer, inflammation and viral replication [1]. The bromodomain structure consists of approximately 110 residues folded into a bundle of four left-handed α helices (αZ , αA , αB and αC). Two variable loops termed ZA loop and BC loop, connect the helices and form the Kac binding site [2]. Despite the structural conservation of bromodomains, sequence and structural heterogeneity in the loop regions result in different druggability [3].

The most studied bromodomains are the members of the bromodomain and extra terminal domain (BET) subfamily. Highly potent and specific inhibitors for the BET subfamily have shown therapeutic potential in a number of diseases, particularly in

oncology [4–6]. Outside the BET subfamily, the recent disclosure of chemical probes for bromodomains like CREBBP/EP300 [7–11], BRD7/9 [12–14], BAZ2A/B [15,16], SMARCA2/4 [17], PCAF [18], and ATAD2 [19] will facilitate the elucidation of the biological function and target validation of the non-BET bromodomains.

The bromodomain and plant homeodomain (PHD) finger containing proteins (BRPF1/2/3) are members of subfamily IV. BRPFs contain multiple epigenetic reader domains, including a unique double PHD and zinc finger assembly, a bromodomain and a C-terminal PWWP domain. As a multivalent chromatin regulator, BRPF1 recognizes histone marks via both the bromodomain and the PWWP domain [20]. The BRPF1 bromodomain preferentially binds to multiple acetyl-lysine marks in histone tails including H2AK5ac, H3K14ac, H4K5ac, H4K8ac, and H4K12ac [21]. BRPF1 is a subunit of monocytic leukemic zinc finger (MOZ) histone acetyltransferase (HAT) which acetylates free histones and affects gene transcription. In the MOZ HAT quaternary complex, BRPF1 enhances the acetylation activity of MOZ.

The MOZ HAT is involved in chromosomal translocations process found in a subtype of acute myeloid leukemia (AML) with poor prognosis [22]. The chromosomal translocation in AML leads to the production of fusion proteins in which MOZ is linked to either CREB binding proteins (CBP) [23], or CBP homolog p300 [24], or the transcriptional intermediary binding factor 2 (TIF2) [25]. MOZ fusion proteins cause aberrant expression profile of HOX genes

* Corresponding author.

E-mail address: caflisch@bioc.uzh.ch (A. Caflich).

mediated by the acetylation activity of MOZ during hematopoiesis, which is found to be critical for leukemogenesis [26]. Overall, the emerging body of evidence suggests the potential of BRPF1 as a therapeutic target in leukemia.

To date, only one chemical probe has been disclosed for the BRPF1 bromodomain. The 1,3-dimethylbenzimidazolone scaffold was optimized into a chemical probe for BRPF1 (GSK6853 [27]), and a dual BRPF1-TRIM24 inhibitor (compound 34 in Ref. [28]) (Fig. 1). The recently reported compounds NI-42 and NI-57 bear a structurally different scaffold N-methylquinolin-2-one [29,30]. The compounds NI-42 and NI-57 are pan-BRPF bromodomain inhibitors, showing a biased potency on BRPF1, and less than six-fold selectivity over BRPF2.

As outlined above, current development of BRPF1 chemical probes still focuses on the 1,3-dimethylbenzimidazolone and N-methylquinolin-2-one scaffolds. It would be valuable to develop compounds structurally orthogonal to the reported BRPF1 chemical probes, especially for inhibitors which are selective within the BRPF subfamily, to better elucidate the biological function of BRPF1. In our previous study, several diverse chemotypes targeting BRPF1 were discovered by high-throughput virtual screening and validated by X-ray crystallography [31]. In the present study, based on two previously identified small molecule hits, a hit-to-lead

campaign was carried out using a structure-based virtual screening strategy. Two series of low micromolar inhibitors were identified which exhibit good selectivity within and outside the subfamily IV bromodomains. Isothermal titration calorimetry was used to measure thermodynamic parameters of binding and confirm selectivity. Explicit solvent molecular dynamics simulations [32,33] confirmed the stability of the head group of the ligand in the Kac binding site and revealed flexibility of the ligand tail (which is partially exposed to solvent) and part of the ZA loop.

2. Results and discussion

2.1. First pharmacophore search

Taking advantage of the rich structural information from our fragment hits [31], we set out to explore the readily available commercial chemical space by a combination of pharmacophore search followed by substructure search (Fig. 2).

At the beginning of this project, a pharmacophore search [34] using PDB coordinate 5EPS as template led to the identification of 365 molecules that include either a 1-ethyl-2,3-dioxo-4H-quinoxaline or a 1-ethyl-3-methyl-2-oxoquinoxaline core group (see section 4. Experimental). Presumably, a carbonyl group of the

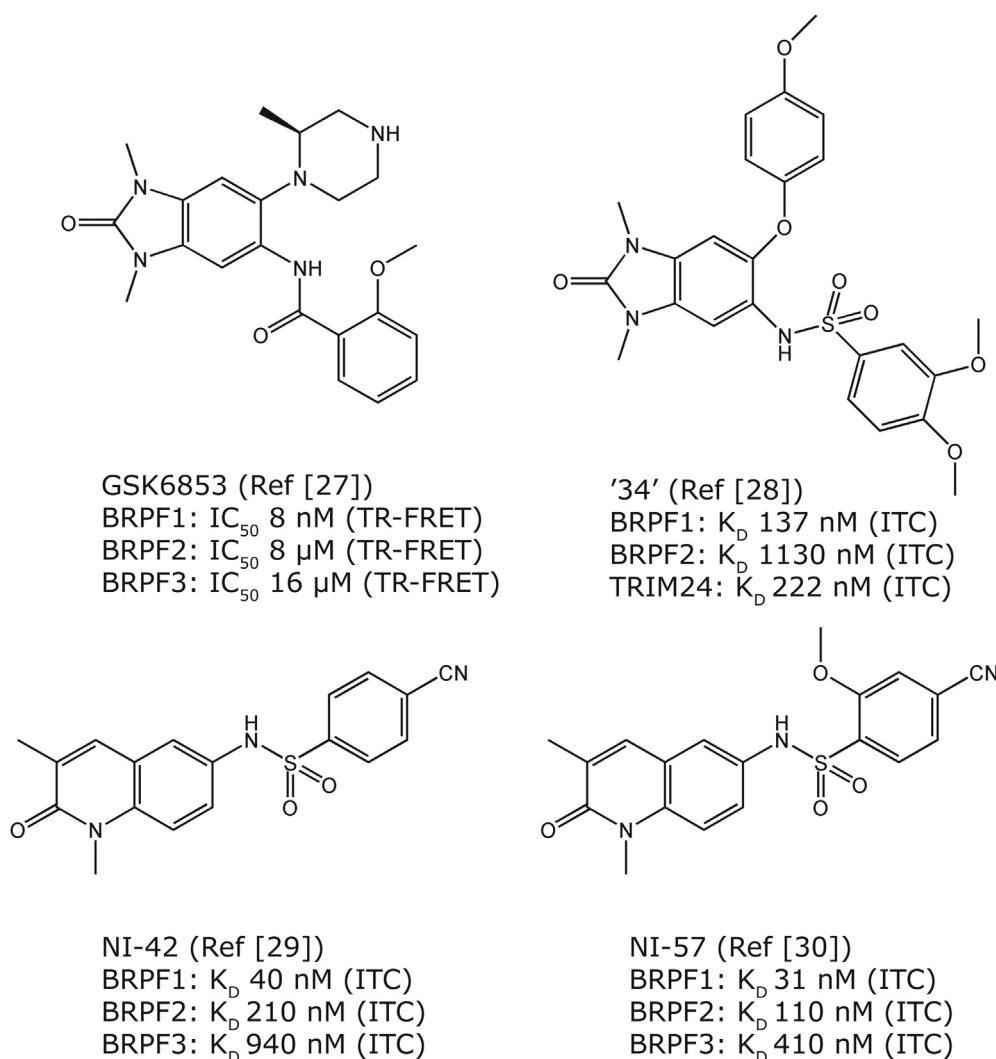


Fig. 1. Representative BRPF1 inhibitors reported previously.

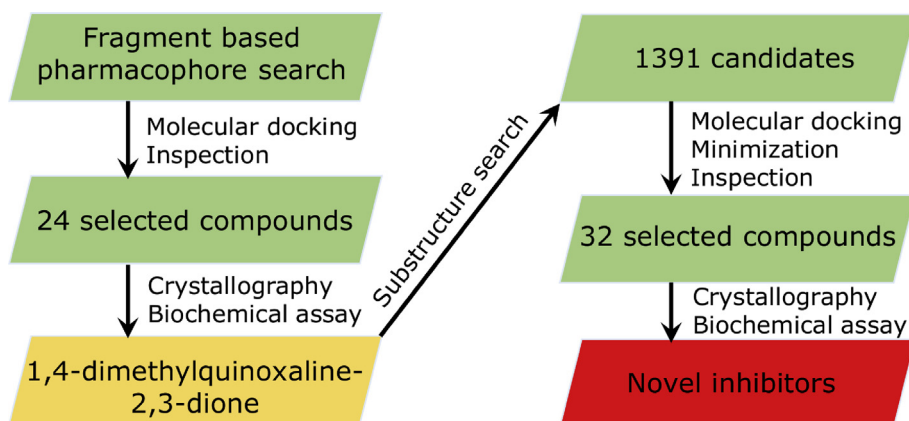


Fig. 2. Flowchart of the discovery of quinoxaline-2,3-dione derivatives.

scaffold acts as the Kac mimetic, which can form a hydrogen bond to the conserved asparagine (Asn708) in BRPF1. Therefore, this key hydrogen bond interaction was used to filter docking poses generated by Autodock Vina [35]. Seven of the 24 selected compounds exhibited K_D values below $50\ \mu\text{M}$ as determined by a competition binding assay [36] (Table 1 and Table S2). Moreover, compounds **2**, **5** and **8** showed good selectivity on BRPF1 against TRIM24 ($K_D > 100\ \mu\text{M}$) and BRD4(1) ($K_D > 100\ \mu\text{M}$) bromodomains. Overall, this series of compounds shows reasonable cLogP values (<3) and have lipophilic efficiency higher than 2.0.

Crystallographic screening (soaking or co-crystallization, see Experimental) was performed to validate the pharmacophore search and pose predicted by docking. Three co-crystals of the BRPF1 bromodomain with compounds **2**, **7** and **8** were solved at resolutions higher than $1.6\ \text{\AA}$ (Table S1). As expected from the docking results (Fig. S1), the quinoxaline head group binds in the Kac pocket with the canonical hydrogen bonding to Asn708 and a buried water molecule bridging to the side chain of Tyr665 (Fig. 3). Interestingly, both of the carbonyl groups on the quinoxaline ring of **2** form hydrogen bond interactions with the bridging water molecule (Fig. 3A). In the crystal structure with compound **2**, the 3-position carbonyl group has an additional hydrogen bond interaction with the SH group of Cys704 which locates at the bottom of the Kac pocket. Furthermore, the NH group of quinoxaline of **2** is involved in a hydrogen bond to the backbone carbonyl of Ile652. Compared to **7** and **8**, the additional methyl group at the amide linker of **2** displaces a conserved water molecule in the binding site. The amide-based linkers occupy different positions in the binding site (Fig. 3D). The tail groups of these compounds pack against the nonpolar part of the side chain of Glu661.

The binding modes of **2**, **7** and **8** show two orientations of the quinoxaline scaffold: the ethyl group of **2** points towards the side chain of Tyr707 in the BC loop, whereas the ethyl group of **7** and **8** points towards the side chains of Ile652 and Phe653 in the so-called NIF shelf (i.e., the Asn651-Ile652-Phe653 triad) in the N-terminal segment of the ZA loop. The structural overlap of the crystal structures of BRPF1 in the complex with compounds **2**, **7**, and **8** shows that a modified quinoxaline with methyl or ethyl groups at both positions 1 and 4 could be accommodated in the binding pocket.

To test this hypothesis, we tried to crystallize BRPF1 with the fragment **9**, i.e., 1,4-dimethylquinoxaline-2,3-dione (Table 2). The co-crystal structure at resolution of $1.5\ \text{\AA}$ shows clear electron density for fragment **9** (Fig. 3E). Similarly to the binding mode of compound **2**, both of the carbonyl groups on the quinoxaline ring of the fragment are involved in hydrogen bonding to the structurally

conserved water molecule that acts as bridge towards the hydroxyl group of the evolutionary conserved Tyr665. The hydrogen bond interactions with the side chains of Cys704 and Asn708 are also present. One of the two methyl groups on the quinoxaline ring forms van der Waals interactions with the side chain Ile652 and Phe653 of the NIF shelf.

2.2. Substructure search

Fragment **9** provided a starting point for a substructure search. Nearly 1400 compounds were retrieved via substructure search in the ZINC database [37], for which either methyl or ethyl groups are present at positions 1 and 4 on the quinoxaline core, and varied tail groups at positions 6 and 7. To in silico screen these candidate compounds, flexible docking was performed with Autodock Vina [35] and docking poses were filtered using the structure of the complex with compound **9** as reference. Next, binding poses were refined by energy minimization with CHARMM [38] using a similar protocol as in a recent work [39], and ranked with a knowledge-based scoring function DSX [40]. The top 1596 poses (of a total of 3967 poses) were inspected visually, and 32 compounds with favorable lipophilic contacts and hydrogen bonds were purchased for binding affinity measurements by BROMOscan and AlphaScreen [41]. Like before, a crystallographic screening was performed by both soaking and co-crystallization methods. Of the 32 molecules screened, compounds **13**, **16**, **21**, **26** and **36** showed binding to the Kac pocket by co-crystallization and could be unambiguously built into the electron density map.

Crystal structures of BRPF1 with **13**, **16**, **21**, **26** and **36** were solved at resolutions higher than $1.8\ \text{\AA}$ (Table S1). As expected, the quinoxaline head groups bind to the Kac pocket in a similar way as for the parent scaffold **9** (Fig. 4). The docking approach successfully predicted the crystallographic poses, as for **13**, **16**, **21** and **26**, the docked poses show root-mean-square deviation (RMSD) less than $1.6\ \text{\AA}$ with respect to the binding mode in the crystal structure (Fig. S1). In all cases, the carbonyl group at position 3 can simultaneously form hydrogen bond interactions with Asn708, Cys704 and water bridging to the conserved Tyr665. As for the other carbonyl, it acts as hydrogen bond acceptor for the NH_2 of Asn708.

The tail groups show interesting binding features in the crystal structures. The phenyl ring of **13** and **21** and aromatic ring of **16** and **26** form an edge-to-face π - π stacking interaction with the so-called gatekeeper residue which is Phe714 in BRPF1. The isobutyl group of **13** and **21** and the saturated ring of the tetralin in compounds **16** and **26** occupy a hydrophobic groove located between the side chains of Ile 713 and Phe714. The substituents at the position 6 of

Table 1
Validation of pharmacophore search results. 2D structures and binding affinity of 1-ethyl-2,3-dioxo-4H-quinoxaline and 1-ethyl-3-methyl-2-oxoquinoxaline derivatives.

Cpd	2D structure	BROMOscan K_D (μM) ^a			cLogP ^b [LiPE ^c]	PDB Code
		BRPF1	TRIM24	BRD4(1)		
1		16	ND	ND	2.46 [2.34]	
2		17	>100	>100	1.96 [2.81]	505A
3		36	ND	ND	2.56 [1.88]	
4		45	ND	ND	2.11 [2.24]	
5		19	>100	>100	2.71 [2.01]	
6		18	ND	ND	1.80 [2.94]	
7		>50	ND	ND	–	505F
8		20	>100	>100	1.29 [3.41]	5055

^a BROMOscan is a competition binding assay. The K_D values were measured in duplicates.

^b Calculated with ChemAxon (www.chemaxon.com).

^c Lipophilic efficiency is calculated as $\text{LiPE} = \text{pIC}_{50} - \text{cLogP}$. ND indicates data not determined.

the quinoxaline point towards the NIF shelf. Furthermore, the morpholine group in **21** and **26** contacts a backbone carbonyl of Gly650 via a water mediated hydrogen bond.

The crystal structures can be employed to interpret the structure-activity relationship for this series of compounds. The substituent at position 6 seems crucial in increasing binding potency, as evidenced by some pairwise comparisons (Table 2). For example, by introduction of a morpholine group, potency of **21** is significantly increased as compared to **13** which has a pyrrolidine group, as observed in both the BROMOscan (K_D of 18 μM and 1.8 μM for compounds **13** and **21**, respectively) and AlphaScreen assay (IC_{50} of 11 μM and 1.9 μM). Similarly, improved potency was observed for **24** (IC_{50} of 3.6 μM in AlphaScreen) as compared to **10** ($\text{IC}_{50} = 10.5 \mu\text{M}$). However, compounds bearing 6-position morpholine or piperidine groups showed similar affinity. For instance, **16** (piperidine group at position 6) shows an IC_{50} of 1.7 μM in AlphaScreen and **26** (piperidine) has an IC_{50} of 3.4 μM . As seen from the crystal structure of BRPF1/**16**, the position 2 carbonyl of **16** provided an additional hydrogen bonding interaction with the

bridging water molecule, which may compensate for the loss of the interaction with Gly650, as compared to **26**. Overall, for this compound series with the sulfonamide linker, it seems bulkier group at position 6 may bring higher potency. For future lead optimization, it might be beneficial to directly contact Gly650 by introduction of a modified 6-position substituent.

Due to a single crystal structure with compound **36** ($\text{IC}_{50} = 16 \mu\text{M}$) and the discrepancy between BROMOscan and AlphaScreen assay results (e.g., compound **32** has a $K_D > 50 \mu\text{M}$ and $\text{IC}_{50} = 4.4 \mu\text{M}$, respectively), it is difficult to discuss the structure-activity relationship for the compounds **28–36** which have an amide linker. We propose that for this category of compounds, the amide and the linked group may stack against the flexible side chain of Glu661, as exemplified by the crystal structure of BRPF1/**36** (Fig. 4E). Interestingly, it seems that heterogeneous 6-position groups can be employed for this series, for instance, a diethylamino group in **28** ($\text{IC}_{50} = 0.77 \mu\text{M}$) and a methyl-piperidine substituent in **32** ($\text{IC}_{50} = 4.4 \mu\text{M}$) both result in potent compounds.

Isothermal titration calorimetry was used to characterize the

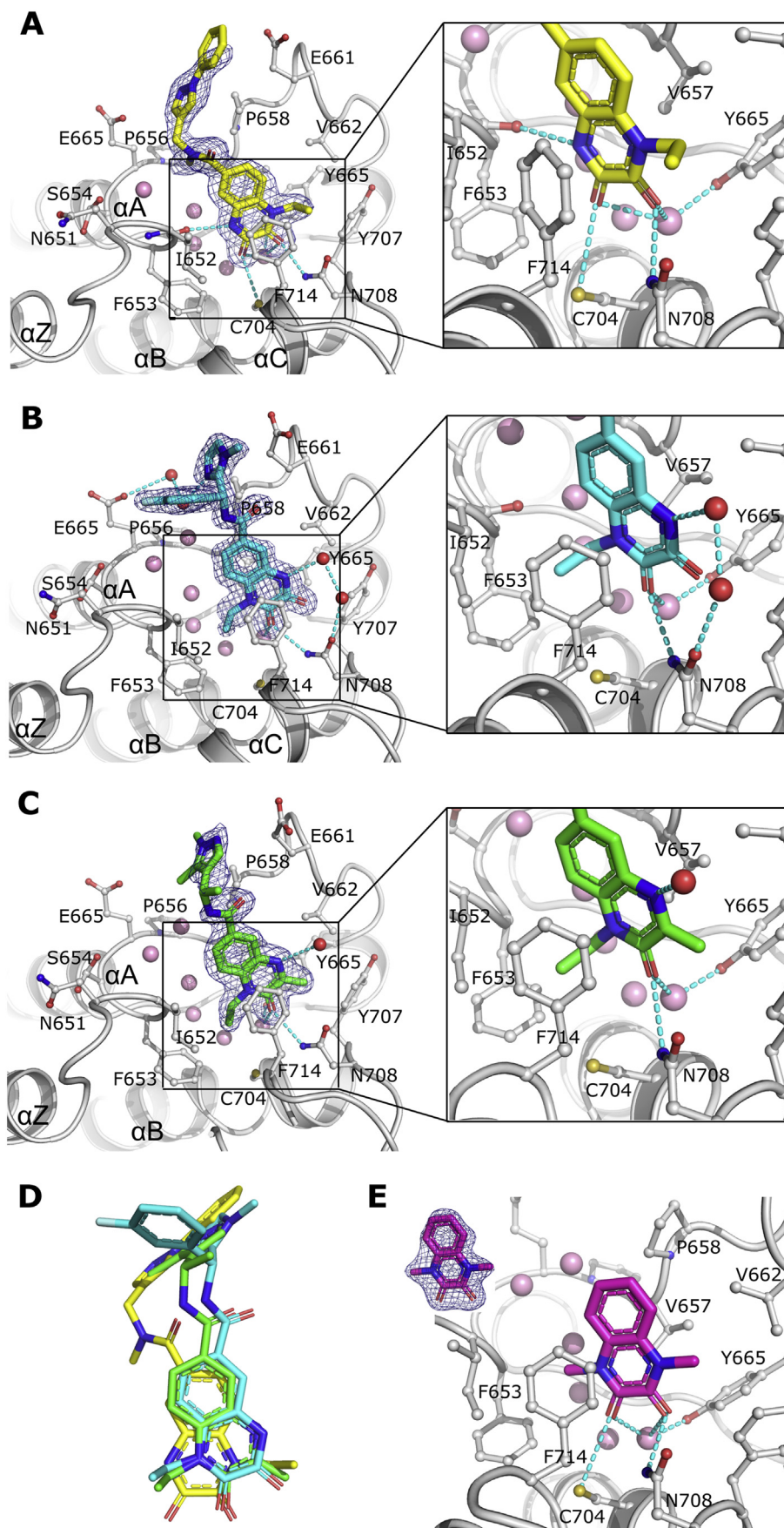


Fig. 3. Co-crystal structures of the BRPF1 bromodomain in complex with compounds **2** (A), **7** (B), **8** (C), and **9** (E). The conserved water molecules and other water molecules involved in ligand binding are shown as pink and red spheres, respectively, while hydrogen bonds are shown by dashed lines using a threshold on hydrogen bond donor and acceptor of 3.5 Å. The $2F_o - F_c$ electron density maps are shown in blue mesh at a contour level of 1.0 sigma. For compounds **8** and **9**, the electron density maps are shown at 0.8 sigma. (D) Superimposition of binding poses of compounds **2** (yellow), **7** (cyan) and **8** (green). (For interpretation of the references to colour in this figure legend, the reader is referred to the Web version of this article.)

binding thermodynamics of compound **21** (Fig. 5C). A K_D value of 2.7 μM was obtained, which is in good agreement with the BROMOScan (K_D of 1.8 μM) and AlphaScreen (IC_{50} of 1.9 μM) assay results. The ITC data indicated that binding of **21** to the BRPF1 bromodomain is mainly enthalpic, with an enthalpy change of $-8.5 \text{ kcal mol}^{-1}$ and a small entropy penalty of $0.9 \text{ kcal mol}^{-1}$. Furthermore, ITC measurements of the binding of compound **26** showed similar thermodynamic characteristics, with a K_D of 2.5 μM , ΔH of $-8.6 \text{ kcal mol}^{-1}$, and $-\Delta S$ of $0.9 \text{ kcal mol}^{-1}$ (Fig. S2). These measurements suggest optimal hydrogen bonding and van der Waals interactions between the BRPF1 bromodomain and this series of compounds. Overlap to the apo structure shows only minor conformational changes in BRPF1 upon binding of **21** and its analogues (Fig. 4F).

Taken together, the substructure search using fragment **9** and information on its binding mode has led to the discovery of a series of compounds with low micromolar affinity and favorable lipophilic efficiency. In total 11 compounds have IC_{50} below 10 μM , 10 compounds exhibit LiPE higher than 3.0, and even LiPE higher than 4.0 for compounds **19**, **22**, and **23**.

2.3. Selectivity

We next analyzed the selectivity profile of compound **21** by the AlphaScreen assay (Fig. 5D). The assay results showed that **21** has negligible activity on subfamily IV members BRPF2, BRPF3, and ATAD2 bromodomains, and marginal activity ($\text{IC}_{50} = 204 \mu\text{M}$) on BRD9 bromodomain. Moreover, **21** was inactive on promiscuous BRD4(1) (subfamily II) and CREBBP (subfamily III) bromodomains. In addition, binding of **21** to the BRPF2 bromodomain was too weak to record the thermodynamic signature in an ITC measurement (Fig. 5C, red curves). To elucidate the structural basis of the selectivity of **21**, the crystal structure of BRPF1/**21** was aligned with apo BRPF2 and BRD4(1) bromodomain structures (Fig. 5A and B, respectively). The favorable van der Waals contacts between the sulfonamide linker of **21** and Pro658 in BRPF1 are absent in BRPF2, as the side chain of the corresponding residue in BRPF2 (Ser592) points outwards the binding site. The structural overlap with BRD4(1) suggests that steric collisions may occur between the morpholine ring of **21** and Trp81 (W of the WPF shelf) in BRD4(1). Furthermore, the binding pocket of BRD4(1) is narrower than that of BRPF1, especially for the ZA loop segment surrounding Leu92, which may also cause steric clashes with **21**. Sequence alignment of BRPF1 bromodomain with other bromodomains tested in the selectivity panel provided additional information (Fig. S3). First, the gatekeeper in the BRPF subfamily members is a phenylalanine, while it is a smaller hydrophobic residue (valine or isoleucine) or a tyrosine in other bromodomains, for which the T-shaped π - π stacking with **21** cannot be formed. Secondly, Pro658 in BRPF1 corresponds to polar residues in other bromodomains (except TRIM24), and as such the lipophilic contacts with **21** are not possible.

2.4. Molecular dynamics simulations

To further investigate the binding mode and selectivity of compound **21**, three independent molecular dynamics runs were performed for its complex with the BRPF1 bromodomain and three with the BRPF2 bromodomain. The binding mode of **21** in BRPF1 is stable in the Kac pocket during the 500 ns simulation time (Fig. 6A). Conversely, **21** was not stable in BRPF2 and in one of the three MD runs it escaped from the binding pocket within the first 100 ns and there was no re-binding. The crucial hydrogen bond interaction between the NH group of Asn708 and the 3-position carbonyl group of **21** was present in 90% of the simulation time for BRPF1

while it broke in the first 100 ns in two of the three runs with the BRPF2 complex.

Besides reporting on the main intermolecular interactions, the molecular dynamics trajectories shed light on the orientation and intrinsic flexibility of the tail group. The dihedral angle distribution of the sulfonamide linker shows that **21** is mainly in a conformation with the isobutyl phenyl group projecting towards the BC loop, and sporadically this group flipped to contact the ZA loop residues (red histograms in Fig. 6B). The simulation of **21** free in solution, i.e., in the unbound state (blue histogram in Fig. 6B), showed that the most populated orientation of the sulfonamide linker is the same as in the complex with BRPF1. As for the X-ray structure, the dihedral angle of the sulfonamide is within the main state observed in the MD simulations of the free (and bound) state. Thus, compound **21** is not strained in its bound conformation observed along the MD simulations and in the X-ray structure. Concerning the relative flexibility of the BRPF1 binding site, the ZA loop region showed the largest flexibility during the simulations (Fig. S4), particularly for the segment Leu659-Ser660-Glu661 (Fig. S5). The plasticity of the ZA loop is consistent with previous simulation studies [42,43]. A bulkier substituent and/or a functional group that stacks against the flexible Glu661 side chain might reduce the flexibility of the ZA loop but it is not possible to predict if the resulting entropic penalty would be fully balanced by an enthalpic gain, i.e., additional favorable interactions.

2.5. Cellular assays

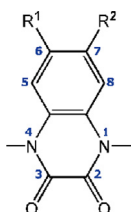
For measuring the cellular efficacy of this series of compounds, we selected compound **26**, which has higher solubility than **21** in the preliminary assay (data not shown). Cell viability was evaluated on acute myeloid leukemia cell lines THP-1 and HL-60. Compound **26** showed growth inhibition in THP-1 cells in a dose-response manner with an EC_{50} of 32 μM , while it displayed no obvious toxicity to normal fibroblast cell line BJ (Fig. 7). In contrast to the THP-1 cell with MLL translocation, **26** showed little effect on non-MLL-rearranged acute leukemia cell line HL-60 in the cell viability assay (data not shown). These observations are in line with a previous study [29] which reported that AML cell lines exhibiting MLL translocation are sensitive to inhibition of BRPF1. However, further optimization of potency is required for further investigations of the mechanism of action of this series of compounds in leukemia cells.

2.6. Second pharmacophore search; discovery of 2,4-dimethyl-oxazole derivatives

From another pharmacophore search [34] based on PDB structure 5EVA (N-methylpyrazole-based compound **19** of Ref. [37]), we identified compounds **42** and **43** (Table 3). We note that these two compounds bear a 2,4-dimethyl-oxazole head, which is different from the 3,5-dimethyl-isoxazole widely used as scaffold in BET bromodomain inhibitor [44–47]. Compound **42** exhibited a K_D of 3.5 μM in BROMOScan assay and IC_{50} of 30.6 μM in AlphaScreen assay for the BRPF1 bromodomain and no measurable binding to the TRIM24 and BRD4(1) bromodomains. Compound **43** showed substantially weaker affinity than **42**.

To validate the pharmacophore model, co-crystal structures of BRPF1 with **42** and **43** were obtained. BRPF1/**42** was solved in two different space groups (Fig. 8 and Table S1). In both cases the 2,4-dimethyl-oxazole head is positioned at the bottom of the Kac site, with the nitrogen atom on it forming hydrogen bonds with Asn708 and the bridging water molecule. The thiazole group stack against Pro658. The tail group 3,5-dimethyl-piperidine show different orientations in two crystal forms; it either points to the ZA channel

Table 2
2D structures and assay results of the 2,3-dioxo-quinoxaline derivatives.



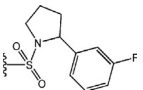
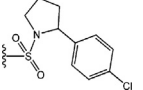
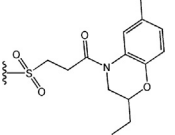
Cpd	R ¹	R ²	BROMOScan			AlphaScreen		
			BRPF1 %Ctrl ^a	TRIM24 %Ctrl ^a	BRPF1 K _D (μM)	BRPF1 IC ₅₀ (μM)	cLogP ^b [LiPE ^c]	PDB Code
9	H	H	ND	ND	ND	>400	—	5O4T
10			43 @100 μM	72 @100 μM	ND	10.5	3.48 [1.50]	
11			17 @100 μM	84 @100 μM	ND	ND	—	
12			3.1 @100 μM	86 @100 μM	ND	8.7	3.35 [1.71]	
13			0 @100 μM	94 @100 μM	18 (n = 2)	11.0	3.05 [1.91]	5OV8
14			3.9 @75 μM	100 @75 μM	11 (n = 2)	ND	1.49 [3.47]	
15			9.9 @100 μM	97 @100 μM	ND	>10	—	
16			12 @100 μM	75 @100 μM	ND	1.7	3.26 [2.51]	5MWG
17			41 @100 μM	74 @100 μM	ND	3.4	2.48 [2.98]	
18			22 @100 μM	82 @100 μM	ND	ND	—	
19			ND	ND	ND	4.4	1.13 [4.22]	
20			4.1 @50 μM	90 @50 μM	33 (n = 2)	ND	1.18 [3.30]	
21			8.4 @100 μM	79 @100 μM	1.8 (n = 2)	1.9 (n = 4)	2.43 [3.29]	5MWH
22			11 @100 μM	84 @100 μM	ND	2.0 (n = 2)	1.41 [4.29]	

(continued on next page)

Table 2 (continued)

Cpd	R ¹	R ²	BROMOscan			AlphaScreen		
			BRPF1 %Ctrl ^a	TRIM24 %Ctrl ^a	BRPF1 K _D (μM)	BRPF1 IC ₅₀ (μM)	cLogP ^b [LiPE ^c]	PDB Code
23			ND	ND	ND	5.4	1.18 [4.08]	
24			ND	ND	ND	3.6	2.85 [2.59]	
25			ND	ND	ND	10.1	1.69 [3.30]	
26			ND	ND	ND	3.4	2.19 [3.27]	5O4S
27			23 @100 μM	77 @100 μM	ND	23.6	3.47 [1.16]	
28			1.6 @25 μM	96 @25 μM	9.7 (n = 2)	0.77	2.12 [3.99]	
29			ND	ND	ND	>200	–	
30			13 @100 μM	86 @100 μM	>20 (n = 2)	27.0	1.81 [2.76]	
31			49 @50 μM	100 @50 μM	ND	ND	–	
32			0 @50 μM	91 @50 μM	>50 (n = 2)	4.4	2.90 [2.46]	
33			46 @25 μM	97 @25 μM	>25 (n = 2)	ND	–	
34			ND	ND	ND	22.3	3.08 [1.57]	
35			91 @25 μM	97 @25 μM	ND	ND	–	
36			55 @20 μM	100 @20 μM	7.1 (n = 2)	16	1.23 [3.56]	5MWZ
37	H		68 @100 μM	94 @100 μM	ND	ND	–	
38	H		81 @50 μM	82 @50 μM	ND	ND	–	

Table 2 (continued)

Cpd	R ¹	R ²	BROMOscan			AlphaScreen		
			BRPF1 %Ctrl ^a	TRIM24 %Ctrl ^a	BRPF1 K _D (μM)	BRPF1 IC ₅₀ (μM)	cLogP ^b [LiPE ^c]	PDB Code
39	H		86 @75 μM	81 @75 μM	ND	ND	–	
40	H		ND	ND	ND	>200	–	
41	H		ND	ND	ND	>200	–	

^a The single-dose value is the percentage of remaining binding of the competitor molecule with respect to DMSO solution at the compound concentration shown in μM; thus lower values indicate stronger binding of the compounds.

^b Calculated with ChemAxon.

^c Lipophilic efficiency is calculated as LiPE = pIC₅₀ - cLogP. The AlphaScreen IC₅₀ values are used for the pIC₅₀, except for compounds **14** and **20** for which the BROMOscan K_D value was employed as the AlphaScreen was not performed. ND indicates data not determined. Compound **36** has N-ethyl substitutions instead of N-methyl.

or the NIF shelf (Fig. 8A and B). Interestingly, the oxygen atom of the oxazole head, and three nitrogen atoms (viz., the NH group of the amide linker, the thiazole nitrogen, and tertiary amino in the tail group) are involved in a water-mediated hydrogen bonding network with the backbone carbonyl groups of Asn651 and Ile652. In the BRPF1/**43** crystal structure (Fig. 8C), the head group of **43** binds in a similar way as **42**, whereas the water-mediated hydrogen bond with the carbonyl group of Asn651 is lost. Compound **43** has a pyridine ring corresponding to the thiazole of **42**, and a different tail group which occupies the ZA channel. Concerning intra-ligand interactions, an intramolecular hydrogen bond between the oxazole oxygen and the NH group of the amide linker seems to contribute to the stability of the bound conformation of compounds **42** (Fig. 8A and B) and **43** (Fig. 8C).

A substructure search using 2,4-dimethyl-N-(thiazol-2-yl)oxazole-5-carboxamide yielded a single molecule in the ZINC database. Thus, we decided to perform a similarity search which yielded 15 analogues of compound **42** with a Tanimoto coefficient larger than 0.3. These 15 compounds were evaluated using the AlphaScreen assay (Table S4). They all showed weaker potency than **42**, probably due to their head groups which are different from the oxazole of **42**. In the biochemical assays (BROMOscan and AlphaScreen), compound **42** presented good selectivity over TRIM24 and BRD4(1) bromodomains (Table 3). To further analyze potency and selectivity, we measured the interaction of **42** with the bromodomains of BRPF1 and BRPF2 by means of ITC. Compound **42** showed a K_D of 10.9 μM on BRPF1 (which is consistent with the affinity of 3 μM and 30 μM measured by AlphaScreen and BROMOscan, respectively, Table 3) while binding signal was not detected for BRPF2 (Fig. 8F). Similar to **21** and **26**, compound **42** appears to be another 'enthalpic efficient' BRPF1 inhibitor, with ΔH of -7.9 kcal mol⁻¹ and -TΔS of 1.2 kcal mol⁻¹. Crystal structure alignment of the BRPF1/**42** complex with apo BRPF2 clearly shows that the Pro658 is essential for the selectivity over BRPF2 (Fig. 8D), as discussed above for the 2,3-dioxo-quinoxaline derivatives. The structural overlap with the BRD4(1) structure reveals potential clashes of compound **42** with the side chains of Trp81 (in the WPF shelf) and Leu92 (Fig. 8E). These bulky side chains are oriented towards the center of the binding site in BRD4(1) while the corresponding residues in BRPF1, Asn651 and Glu661, respectively, point outside.

3. Conclusions

Our previous high-throughput fragment docking campaign [31] paved the way for the present structure-based hit-optimization study. Pharmacophore and substructure searches combined with orthogonal binding assays and X-ray crystallography have led to the identification of a series of 1,4-dimethyl-2,3-dioxo-quinoxaline derivatives, which are structurally different from previously reported BRPF1 bromodomain inhibitors. Some of these compounds showed low micromolar inhibitory activity towards the BRPF1 bromodomain, as confirmed by both biochemical and biophysical assays. Among them, **21** is a 2-μM ligand of the BRPF1 bromodomain with >100-fold selectivity over other bromodomains. Co-crystal structures of BRPF1 with this series of compounds revealed interesting binding features, e.g., a water-bridged hydrogen bond to the carbonyl of Gly650 in the ZA loop. Moreover, the X-ray structures provided structural insights into the origin of selectivity and helped to explain the structure-activity relationship. Molecular dynamics simulations were used to investigate the binding pose of **21** to BRPF1 and its flexibility. The anti-proliferative activity on acute myeloid leukemia cell lines was confirmed by cell viability assay with **26**.

From another pharmacophore search, we discovered compound **42** which bears a 2,4-dimethyl-oxazole scaffold. The selective inhibition of **42** on BRPF1 over other bromodomains was demonstrated by both biochemical assay and isothermal titration calorimetry. Crystallographic study showed extensive hydrogen bond interactions formed in the Kac pocket of BRPF1 upon binding of **42**. The chemotypes discovered in the present study exhibit favorable physicochemical properties, for instance, three of the 1,4-dimethyl-2,3-dioxo-quinoxaline derivatives have lipophilic efficiency higher than 4.0. Moreover, the compounds **21**, **26**, and **42** show enthalpy-driven binding in isothermal titration calorimetry measurements, which makes them suitable candidates for optimization [48].

Taken together, a total of 74 small molecules identified in silico were evaluated by biochemical and/or biophysical assays. Of these 74 small molecules, 57 compounds originated from the pharmacophore searches that made use of the crystal structure of the BRPF1 bromodomain in the complex with 1-methyl-2-oxo-4H-

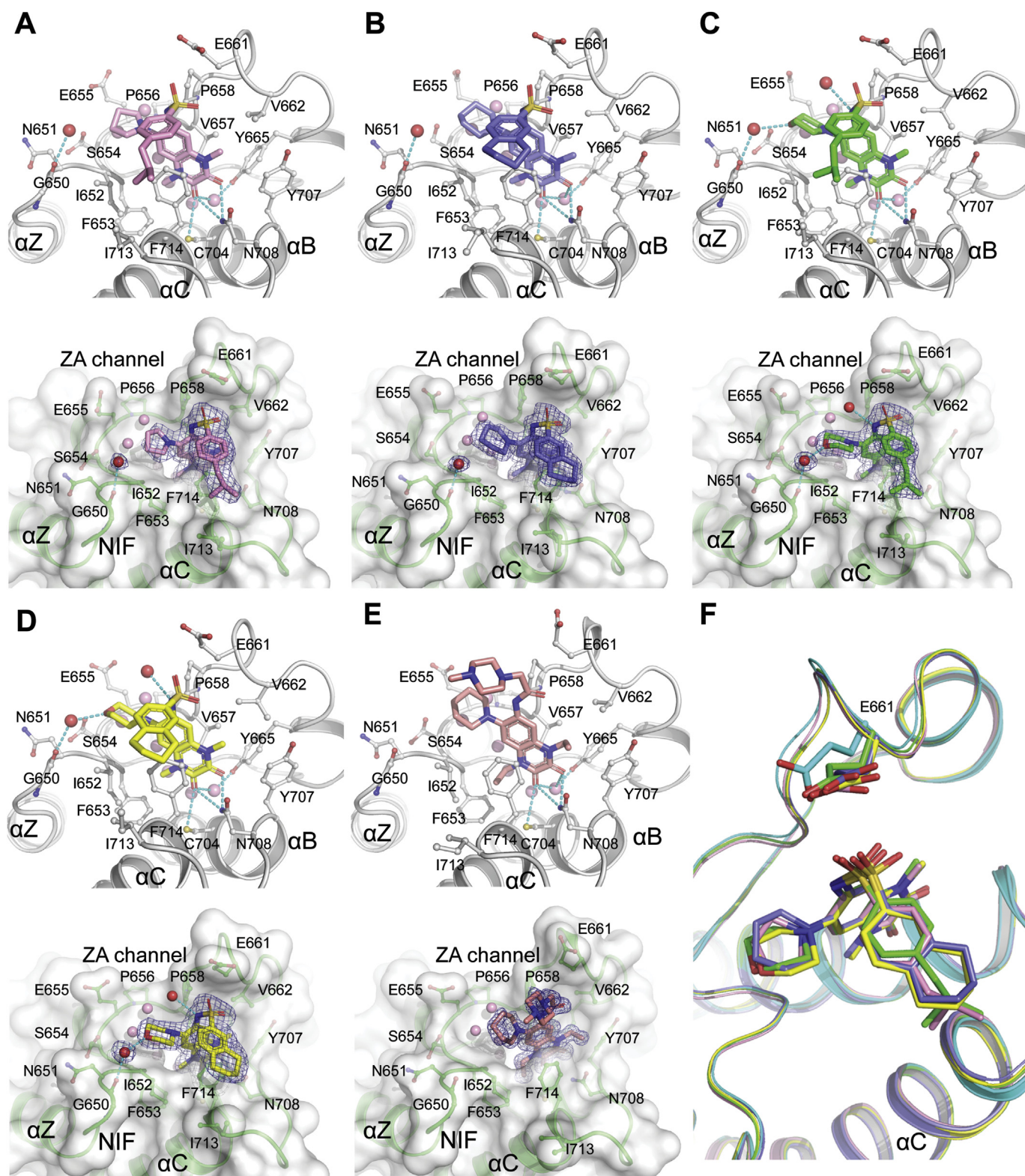


Fig. 4. Co-crystal structures of BRPF1 bound to **13** (A), **16** (B), **21** (C), **26** (D), and **36** (E). The conserved water molecules and other water molecules involved in ligand binding are shown as pink and red spheres, respectively, while hydrogen bonds are shown by dashed lines. The 2Fo - Fc electron density maps are shown in blue mesh at a contour level of 1.0 sigma. (F) Overlap of the complex structures of BRPF1/**13** (pink), BRPF1/**16** (slate), BRPF1/**21** (green), BRPF1/**26** (yellow), and apo BRPF1 4LC2 (cyan). (For interpretation of the references to colour in this figure legend, the reader is referred to the Web version of this article.)

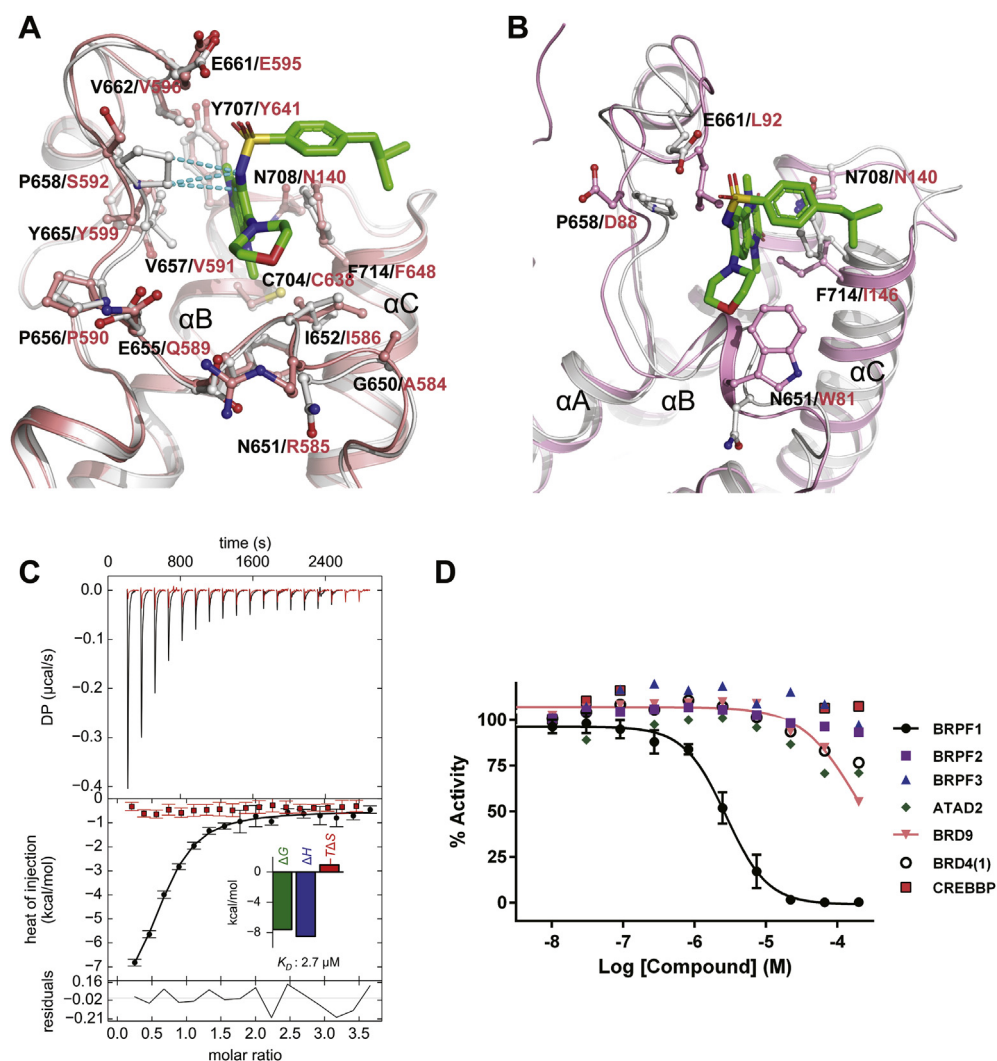


Fig. 5. Selectivity profile of compound **21**. (A) Structural comparison of BRPF1/**21** (white) with apo BRPF2 PDB code 3RCW (salmon). Dashed lines emphasize van der Waals contacts with the side chain of Pro658 in BRPF1 which corresponds to Ser592 in BRPF2 (see text). (B) Structural comparison of BRPF1/**21** (white) with apo BRD4(1) structure 2OSS (pink). (C) Thermodynamic characterization of interactions of **21** with BRPF1 (black) and BRPF2 (red) by ITC. Thermographs, fit of integrated data and fit residuals are shown in the top, middle and bottom panel, respectively. (D) Compound **21** was tested by means of AlphaScreen on bromodomains of BRPF1, BRPF2, BRPF3, ATAD2, BRD9, BRD4(1) and CREBBP. Error bars indicate SEM. Binding is not observed for the off-targets even at a 200 μM concentration of compound **21**. (For interpretation of the references to colour in this figure legend, the reader is referred to the Web version of this article.)

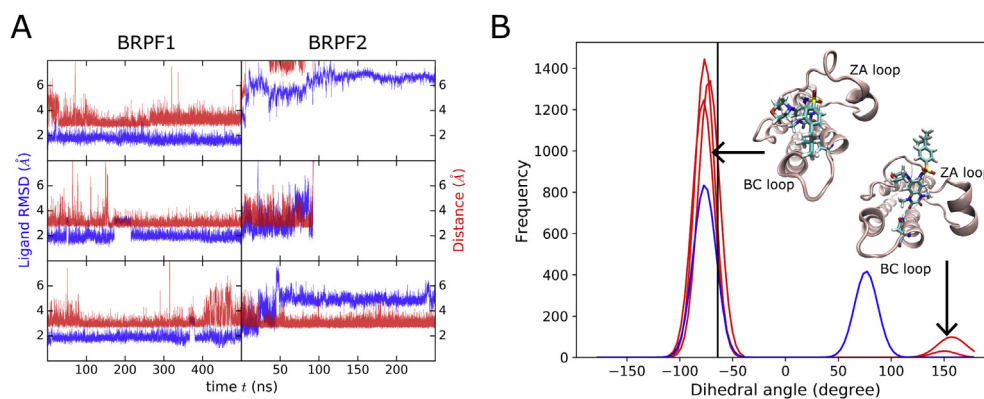


Fig. 6. MD simulations of **21** in the complex with BRPF1 or BRPF2. (A) Time series of RMSD of compound **21** from the initial structure (blue) and distance between N_5 atom of Asn708 and 3-position oxygen atom of **21** (red). Three independent MD runs were started with randomly assigned velocities for the complex with BRPF1 (left) and BRPF2 (right). (B) Histograms of the dihedral angle distribution of the sulfonamide linker of compound **21** in BRPF1 (red) or water (blue). Insets show the conformations of **21** in BRPF1. The vertical line indicate the sulfonamide dihedral angle of -64° in the crystallographic pose (PDB code 5MWH). (For interpretation of the references to colour in this figure legend, the reader is referred to the Web version of this article.)

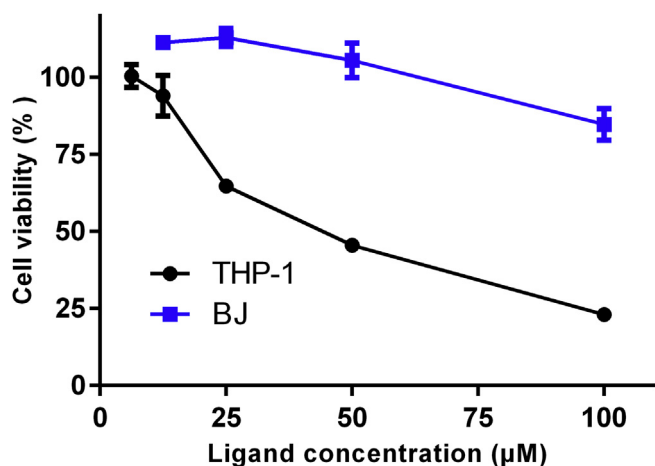


Fig. 7. Cell viability assay of **26** in leukemia cell line THP-1 and normal human fibroblast cell line BJ. The cells were treated with **26** for 72 h. Data points are triplicates and error bars represent SEM.

quinoxaline (PDB code 5EPS) and 17 compounds from the search using an N-methyl-pyrazole derivative (compound **19** of Ref. [31]; PDB code 5EVA), respectively. The pharmacophore and substructure searches were restricted to the purchasable compounds. Since the chemical diversity of the purchasable derivatives is limited it was not possible to reach low nanomolar potency which usually requires optimization by chemical synthesis of derivatives [11,49,50]. The main goal of this work was the identification of novel and selective BRPF1 ligands with structural information on their binding mode. Towards this goal, we have solved 12 holo structures of the BRPF1 bromodomain, nine complexes of BRPF1 with 1,4-dimethyl-2,3-dioxo-quinoxaline derivatives and three complexes with 2,4-dimethyl-oxazole derivatives. We propose the newly identified chemotypes and their structural information as attractive starting points for further development by medicinal chemistry.

4. Experimental

4.1. In silico screening

Two BRPF1 complex structures 5EPS and 5EVA were used for pharmacophore search with ZINCPharmer [34]. The coordinate set 5EPS contains a fragment 3,4-dihydro-1-methylquinoxalin-2(1H)-

one, of which the carbonyl group on the quinoxaline ring was defined as hydrogen bond acceptor, the hydrophobic methyl group and the aromatic benzene are also included in the pharmacophores. In 5EVA, BRPF1 is complexed with a compound that bears a 1-methyl-pyrazole head. Similar to the aforementioned fragment, the methyl group on the pyrazole ring was used as hydrophobic group and the nitrogen atom served as hydrogen bond donor. The carboxamide and the aromatic difluorophenyl group were also used as pharmacophores.

Pharmacophore search based on the structure 5EPS revealed a series of compounds that possess either a 2,3-dioxo-4H-quinoxaline or a 3-methyl-2-oxoquinoxaline head. In total 365 such analogues were assembled and docked into the 5EPS structure with Autodock Vina after manual removal of the ligand. The conserved six water molecules were kept in the Kac binding site and the Glu661 was set to be flexible during docking. A filter of hydrogen bonding to the conserved Asn708 was applied and 24 compounds with a binding affinity < -6.5 kcal mol⁻¹ were selected from 1753 docking poses for further experimental binding validation.

Substructure search based on fragment **9** was performed against the ZINC database using an RDKit-based python script. The retrieved 1391 compounds were docked into the 5EPS structure with Autodock Vina using same docking settings as described above. Filters of hydrogen bonding to the Asn708, binding affinity more favorable than -6.5 kcal mol⁻¹, and a RMSD calculation within 1 Å using the fragment as reference were applied, resulting in 3967 binding poses from 1174 compounds. These molecules were parameterized with CGenFF [51] which is fully consistent with the CHARMM36 force field. Next the binding poses were refined by energy minimization with CHARMM [38]. The optimized binding poses were rescored with a knowledge-based scoring function DSX [40]. In total 1596 poses from 754 compounds survived when a cutoff of DSX score at -110 was applied. The binding poses were visually inspected and 32 compounds were selected based on chemical structure diversity and availability.

Compounds **42** and **43** were identified by the pharmacophore search with structure 5EVA. The search for compounds similar to **42** was performed against ZINC database using a python script based on RDKit [52]. Totally 16 analogues with Tanimoto coefficient greater than 0.3 were selected for binding assay validation.

4.2. Chemistry

All compounds were purchased from Enamine Ltd. and Chemdiv. Their chemical structure was confirmed by HPLC-MS and proton NMR analysis (Supporting Information).

Table 3
Derivatives of 2,4-dimethyl-oxazole identified in the second pharmacophore search.

Cpd	2D structure	BROMOscan K_D (µM)			AlphaScreen IC_{50} (µM)		ITC			PDB code
		BRPF1	TRIM24	BRD4(1)	BRPF1	BRD4(1)	K_D (µM)	cLogP ^a	LE ^c	
42		3.5 (n = 2)	>50	>50	30.6 (n = 2)	>200	10.9	2.13 [2.83]	0.29	5OWA 6EKQ
43		>75 (n = 2)	ND	ND	ND	ND	ND	–	–	505H

^a Calculated with ChemAxon.

^b Lipophilic efficiency is calculated as LiPE = pIC₅₀ - cLogP, according to the ITC data.

^c Ligand efficiency is calculated as LE = (1.4/HA) × pK_D, according to the ITC data. ND indicates data not acquired.

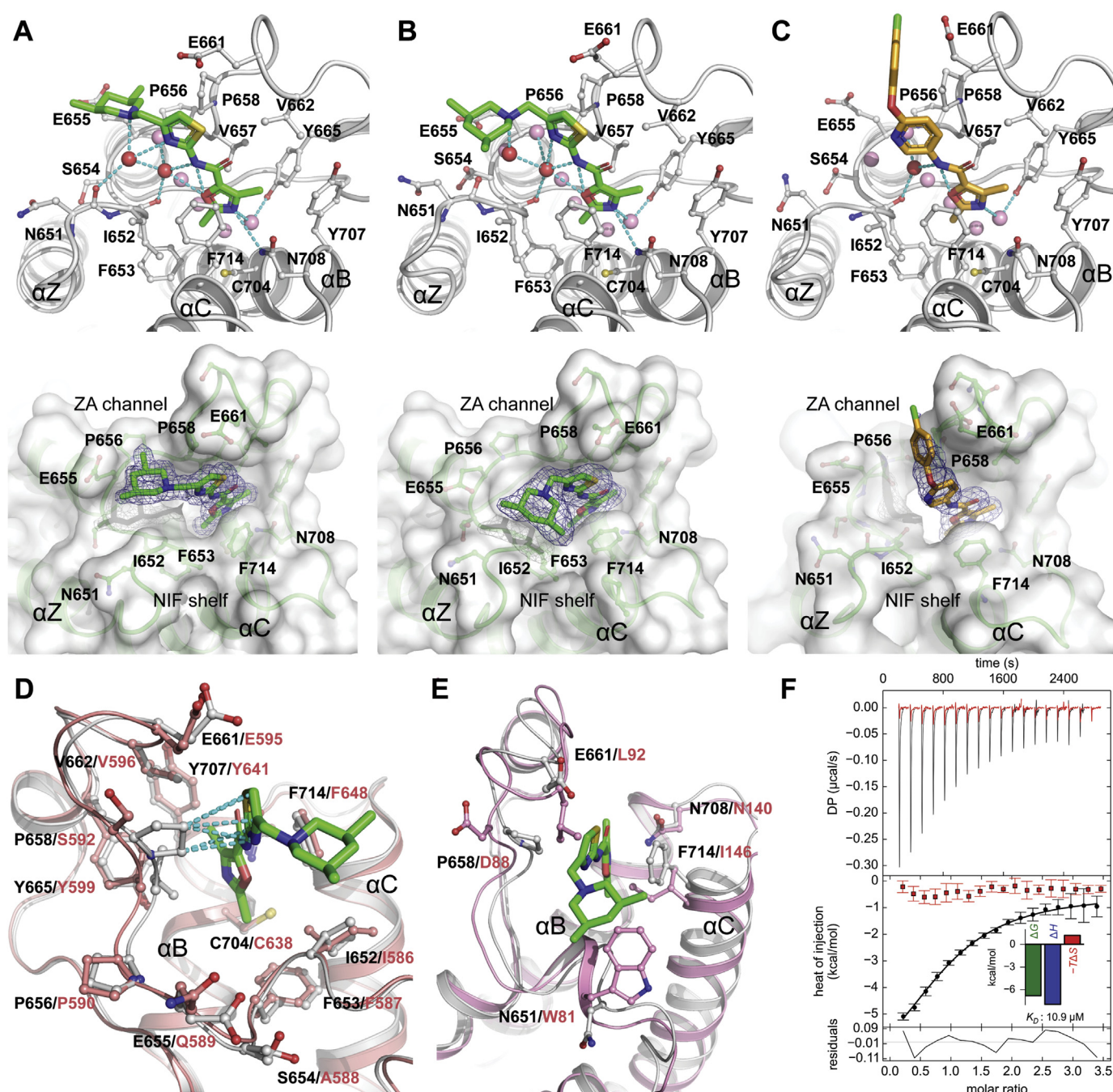


Fig. 8. Co-crystal structures of BRPF1 bound to **42** (A, B) and **43** (C). BRPF1/**42** was crystallized in P2₁ (A) and C2 (B) space groups. The conserved water molecules and other water molecules involved in ligand binding are shown as pink and red spheres, respectively, while hydrogen bonds are shown by dashed lines. The 2Fo – Fc electron density maps are shown in blue mesh at a contour level of 1.0 sigma. (D) Structural comparison of BRPF1/**42** (white) with apo BRPF2 structure 3RCW (salmon). (E) Structural comparison of BRPF1/**42** (white) with apo BRD4(1) structure 2OSS (pink). (F) Thermodynamic characterization of interaction of **42** with BRPF1 (black) and BRPF2 (red) by ITC. Thermographs, fit of integrated data and fit residuals are shown in the top, middle and bottom panel, respectively. (For interpretation of the references to colour in this figure legend, the reader is referred to the Web version of this article.)

4.3. BROMOscan assay

The BROMOscan assay was performed at DiscoverRx. T7 phage strains were used to display bromodomains in an *E. coli* host derived from the BL21 strain. Streptavidin-coated magnetic beads were treated with biotinylated small molecule or acetylated peptide ligands for 30 min at room temperature to generate affinity resins for bromodomain assays. Binding reactions were assembled by combining bromodomains, liganded affinity beads, and test

compounds in 1x binding buffer (17% SeaBlock, 0.33 × PBS, 0.04% Tween 20, 0.02% BSA, 0.004% Sodium azide, 7.4 mM DTT). Test compounds were prepared as 1000 × stocks in DMSO and subsequently diluted 1:10 in monoethylene glycol (MEG) to create stocks at 100 × the screening concentration (resulting stock solution is 10% DMSO/90% MEG). The compounds were then diluted directly into the assays such that the final concentration of DMSO and MEG were 0.1% and 0.9%, respectively. All reactions were performed in polystyrene 96-well plates in a final volume of 0.135 ml.

The assay plates were incubated at room temperature with shaking for 1 h and the affinity beads were washed with wash buffer (1 × PBS, 0.05% Tween 20). The beads were then resuspended in elution buffer (1 × PBS, 0.05% Tween 20, 2 μM non-biotinylated affinity ligand) and incubated at room temperature with shaking for 30 min. The bromodomain concentration in the eluates was measured by qPCR. Binding constants (K_D) were calculated with a standard dose-response curve using the Hill equation. Curves were fitted using a non-linear least square fit with the Levenberg-Marquardt algorithm. Assay results are shown in Table S3 in Supporting Information.

4.4. AlphaScreen assay

The AlphaScreen assay was carried out at Reaction Biology. Recombinant His-tagged bromodomains, test compounds and biotinylated H4(1-21)K5/8/12/16Ac peptide were delivered to a 384-well OptiPlate and incubated at room temperature for 30 min with gentle shaking. Streptavidine donor beads and nickel chelate acceptor beads were added to plates followed by incubation in dark for 60 min with gentle shaking. Recombinant bromodomains, compounds, donor and acceptor beads were prepared as 4 × stock solution in the buffer of 50 mM HEPES-HCl, pH 7.5, 100 mM NaCl, 1 mg/ml BSA, 0.05% CHAPS and 0.5% DMSO. Alpha signal (Ex/Em = 680/520–620 nm) was measured with an EnSpire plate reader. Dose-response curve was fit with GraphPad Prism 6 using a nonlinear regression analysis model.

4.5. Protein production

BRPF1 bromodomain was purified as an N-terminal GST fusion protein in *E. coli* as described previously. Purified protein was changed into ITC buffer (50 mM HEPES, pH 7.5 and 150 mM NaCl) using gel filtration chromatography for the use of ITC measurements. The vector harboring N-terminal 6-His tagged BRPF2 bromodomain was purchased from Addgene (#25342). BRPF2 plasmid was transformed to BL21-CodonPlus competent cells. Protein expression was induced by adding 0.2 mM IPTG to the TB medium when OD₆₀₀ reached 0.6–0.8, followed by overnight culturing at 18 °C. Harvested cells were disrupted using a French Press instrument in the buffer of 50 mM HEPES, pH 7.5, 300 mM NaCl, 10 mM Imidazole, and 5% Glycerol. Lysate was loaded to a nickel affinity column and contaminants were washed away using a buffer of 50 mM HEPES, pH 7.5, 300 mM NaCl, 25 mM Imidazole and 5% Glycerol. Target protein was purified using an elution buffer (50 mM HEPES, pH 7.5, 300 mM NaCl, 250 mM Imidazole and 5% Glycerol). The 6-His tag was removed by TEV protease afterwards. Finally, protein was purified using gel filtration chromatography in the ITC buffer. Protein concentration (A280) was determined using a NanoDrop spectrophotometer.

4.6. Isothermal titration calorimetry (ITC)

ITC experiments were carried out on a Microcal iTC200 instrument (GE Healthcare) at 25 ° with a reference power of 10 μCal/s, while stirring at a speed of 1000 rpm. Compounds were dissolved in DMSO and were diluted into the ITC buffer at appropriate concentrations and equivalent amount of DMSO was added to protein sample. Bromodomains at a concentration of 350–400 μM were injected into cell containing 20–40 μM compounds (reverse titration). An initial control injection of 0.4 μL was applied and 150 s spacing time between injections was set during titrations. Raw data were integrated and baseline corrected using NITPIC [53] and were analyzed with SEDPHAT [54] using a single-site binding model. Thermographs were plotted with GUSI [55]. Thermodynamic

parameters were calculated according to $\Delta G = \Delta H - T\Delta S$, where ΔG , ΔH , and $T\Delta S$ are changes in free energy, enthalpy, and entropy of binding, respectively.

4.7. Crystallization of BRPF1/ligand complexes

BRPF1 bromodomain was co-crystallized with inhibitors by vapor diffusion in hanging drops at 277 K. Co-crystals of BRPF1 with compound **2**, **7**, **8**, **9**, **16**, **21**, **26** and **43** were grown by mixing protein sample at 22 mg/ml concentration with an equal volume of reservoir buffer of 0.1 M Bis-tris propane, pH 6.5, 0.2 M Sodium nitrate, 20% PEG3350. For soaking trials, apo BRPF1 crystals were obtained under the same condition. Co-crystals of BRPF1 with **13** and **36** were obtained using well solution of 0.1 M Bis-Tris propane pH7.4, 5% Ethylene glycol, 0.15 M Sodium nitrate and 25% PEG3350. BRPF1/**42** complex can be crystallized either against reservoir buffer of 0.2 M MgCl₂ and 20% PEG3350 or a buffer of 0.1 M Bis-Tris propane, pH 9.0, 10% Ethylene glycol, 0.15 M Sodium nitrate and 25% PEG3350.

4.8. Structure determination and refinement

Crystals obtained from co-crystallization or soaking were screened for diffraction and data sets were collected at the Swiss Light Source, Paul Scherrer Institute (Villigen, Switzerland), beamlines X06DA and X06SA. Data reduction was performed with XDS [56] and scaled with Aimless [57]. Structures were solved by molecular replacement with Molrep [58] in CCP4 suite [59] using apo BRPF1 structure 4LC2 as a search model. Structures were refined with PHENIX [60] and were manually built with COOT [61] for several rounds. Topology files of compounds were obtained from the PRODRG server [62].

4.9. Molecular dynamics simulations

Molecular dynamics simulations were carried out with GRO-MACS [63] on Cray XC40 compute nodes at Swiss National Supercomputing Center (6900 Lugano, Switzerland). The co-crystal structure of BRPF1 in complex with **21** was used as starting coordinate set with conserved water molecules kept in the binding site. As in previous protein structure-based virtual screening campaigns [64,65] the CHARMM36 force field [66] was used for the parameters of BRPF1, the CGenFF [51] for those of compound **21**, and water was represented by the TIP3P model. All of the simulations were run in a cubic water box with minimum distance between protein and water box edge of 12 Å using periodic boundary conditions. The systems were neutralized by adding Na⁺ and Cl⁻ counter ions and energy minimization was carried out for 10,000 steps. A 100-ps NVT run followed by a 100-ps NPT run were performed to equilibrate the system. The electrostatic interactions were calculated with the particle mesh Ewald algorithm and all bonds were constrained using the LINCS algorithm. Production simulations were carried out with a time step of 2 fs at constant temperature (300 K) and pressure (1 atm). Snapshots were saved every 10 ps and analyzed with built-in GROMACS tools.

4.10. Cell viability assay

AML cell lines THP-1 and HL-60, and normal skin fibroblast BJ were purchased from Shanghai Institute for Biological Science. Cells were maintained in RPMI-1640 medium (THP-1) and DMEM medium (HL-60 and BJ) containing 10% (v/v) fetal bovine serum (FBS), at 37 °C in a humidified atmosphere of 5% CO₂. The growth inhibitory activity of tested compounds were measured using Cell Counting Kit-8 according to manufacturer's instruction (Dojindo

Molecular Technologies). Cells were seeded in 96 well plates in 100 μ L media per well. Compounds and vehicle (DMSO) were added at varying concentrations and cell cultures were incubated 37 °C for 72 h. Optical density at a wavelength of 450 nm was measured using a plate reader (Epoch, BioTek). Dose-response curves were generated and EC₅₀ values were calculated using non-linear regression analysis with GraphPad Prism 6. All measurements were performed at least three times.

Accession code

The coordinate files of BRPF1 in complex with **2** (5O5A), **7** (5O5F), **8** (5O55), **9** (5O4T), **13** (5OV8), **16** (5MWG), **21** (5MWH), **26** (5O4S), **36** (5MWZ), **42** (5OWA and 6EKQ), and **43** (5O5H) have been deposited to the Protein Data Bank. Authors will release the coordinates and experimental data upon article publication.

Notes

The authors declare no conflict of interest.

Associated content

Molecular formula strings for ligands **1–43** (CSV).

Acknowledgments

We thank the staff at Swiss Light Source (beamlines X06SA and X06DA, Paul Scherrer Institute) for their assistance during crystal data collection. We thank Prof. W.L. Zhao, Prof. S.G. Zhu and Dr. Z.H. Su for helpful discussions. We greatly acknowledge financial support by the Swiss National Science Foundation to A.C. (31003A_169007).

Appendix A. Supplementary data

Supplementary data related to this article can be found at <https://doi.org/10.1016/j.ejmech.2018.05.037>.

References

- [1] R. Sanchez, M.M. Zhou, The role of human bromodomains in chromatin biology and gene transcription, *Curr. Opin. Drug Discov. Dev* 12 (2009) 659–665.
- [2] P. Filippakopoulos, S. Picaud, M. Mangos, T. Keates, J.P. Lambert, D. Barsyte-Lovejoy, I. Felletar, R. Volkmer, S. Muller, T. Pawson, A.C. Gingras, C.H. Arrowsmith, S. Knapp, Histone recognition and large-scale structural analysis of the human bromodomain family, *Cell* 149 (2012) 214–231.
- [3] L.R. Vidler, N. Brown, S. Knapp, S. Hoelder, Druggability analysis and structural classification of bromodomain acetyl-lysine binding sites, *J. Med. Chem.* 55 (2012) 7346–7359.
- [4] J.E. Delmore, G.C. Issa, M.E. Lemieux, P.B. Rahl, J. Shi, H.M. Jacobs, E. Kastritis, T. Gilpatrick, R.M. Paranal, J. Qi, M. Chesi, A.C. Schinzel, M.R. McKeown, T.P. Heffernan, C.R. Vakoc, P.L. Bergsagel, I.M. Ghobrial, P.G. Richardson, R.A. Young, W.C. Hahn, K.C. Anderson, A.L. Kung, J.E. Bradner, C.S. Mitsiades, BET bromodomain inhibition as a therapeutic strategy to target c-Myc, *Cell* 146 (2011) 904–917.
- [5] S. Picaud, D. Da Costa, A. Thanasopoulou, P. Filippakopoulos, P.V. Fish, M. Philpott, O. Fedorov, P. Brennan, M.E. Bunnage, D.R. Owen, J.E. Bradner, P. Taniere, B. O'Sullivan, S. Muller, J. Schwaller, T. Stankovic, S. Knapp, PFI-1, a highly selective protein interaction inhibitor, targeting BET Bromodomains, *Canc. Res.* 73 (2013) 3336–3346.
- [6] M.A. Dawson, R.K. Prinjha, A. Dittmann, G. Giotopoulos, M. Bantscheff, W.I. Chan, S.C. Robson, C.W. Chung, C. Hopf, M.M. Savitski, C. Huthmacher, E. Gudgin, D. Lugo, S. Beinke, T.D. Chapman, E.J. Roberts, P.E. Soden, K.R. Auger, O. Mirguet, K. Doehner, R. Delwel, A.K. Burnett, P. Jeffrey, G. Drewes, K. Lee, B.J. Huntly, T. Kouzarides, Inhibition of BET recruitment to chromatin as an effective treatment for MLL-fusion leukaemia, *Nature* 478 (2011) 529–533.
- [7] T.D. Crawford, F.A. Romero, K.W. Lai, V. Tsui, A.M. Taylor, G. de Leon Boenig, C.L. Noland, J. Murray, J. Ly, E.F. Choo, T.L. Hunsaker, E.W. Chan, M. Merchant, S. Kharbanda, K.E. Gascoigne, S. Kaufman, M.H. Beresini, J. Liao, W. Liu, K.X. Chen, Z. Chen, A.R. Conery, A. Cote, H. Jayaram, Y. Jiang, J.R. Kiefer, T. Kleinheinz, Y. Li, J. Maher, E. Pardo, F. Poy, K.L. Spillane, F. Wang, J. Wang, X. Wei, Z. Xu, Z. Xu, I. Yen, L. Zawadzke, X. Zhu, S. Bellon, R. Cummings, A.G. Cochran, B.K. Albrecht, S. Magnuson, Discovery of a potent and selective in vivo probe (GNE-272) for the bromodomains of CBP/EP300, *J. Med. Chem.* 59 (2016) 10549–10563.
- [8] D.A. Hay, O. Fedorov, S. Martin, D.C. Singleton, C. Tallant, C. Wells, S. Picaud, M. Philpott, O.P. Monteiro, C.M. Rogers, S.J. Conway, T.P. Rooney, A. Tumber, C. Yapp, P. Filippakopoulos, M.E. Bunnage, S. Muller, S. Knapp, C.J. Schofield, P.E. Brennan, Discovery and optimization of small-molecule ligands for the CBP/p300 bromodomains, *J. Am. Chem. Soc.* 136 (2014) 9308–9319.
- [9] S. Picaud, O. Fedorov, A. Thanasopoulou, K. Leonards, K. Jones, J. Meier, H. Olzscha, O. Monteiro, S. Martin, M. Philpott, A. Tumber, P. Filippakopoulos, C. Yapp, C. Wells, K.H. Che, A. Bannister, S. Robson, U. Kumar, N. Parr, K. Lee, D. Lugo, P. Jeffrey, S. Taylor, M.L. Vecellio, C. Bountra, P.E. Brennan, A. O'Mahony, S. Velichko, S. Muller, D. Hay, D.L. Daniels, M. Uhr, N.B. La Thangue, T. Kouzarides, R. Prinjha, J. Schwaller, S. Knapp, Generation of a selective small molecule inhibitor of the CBP/p300 bromodomain for leukemia therapy, *Canc. Res.* 75 (2015) 5106–5119.
- [10] A.M. Taylor, A. Cote, M.C. Hewitt, R. Pastor, Y. Leblanc, C.G. Nasveschuk, F.A. Romero, T.D. Crawford, N. Cantone, H. Jayaram, J. Setser, J. Murray, M.H. Beresini, G. de Leon Boenig, Z. Chen, A.R. Conery, R.T. Cummings, L.A. Dakin, E.M. Flynn, O.W. Huang, S. Kaufman, P.J. Keller, J.R. Kiefer, T. Lai, Y. Li, J. Liao, W. Liu, H. Lu, E. Pardo, V. Tsui, J. Wang, Y. Wang, Z. Xu, F. Yan, D. Yu, L. Zawadzke, X. Zhu, X. Zhu, R.J. Sims 3rd, A.G. Cochran, S. Bellon, J.E. Audia, S. Magnuson, B.K. Albrecht, Fragment-based discovery of a selective and cell-active benzodiazepinone CBP/EP300 bromodomain inhibitor (CPI-637), *ACS Med. Chem. Lett.* 7 (2016) 531–536.
- [11] A. Unzue, M. Xu, J. Dong, L. Wiedmer, D. Spiliotopoulos, A. Cafilisch, C. Nevado, Fragment-based design of selective nanomolar ligands of the CREBBP bromodomain, *J. Med. Chem.* 59 (2016) 1350–1356.
- [12] P.G. Clark, L.C. Vieira, C. Tallant, O. Fedorov, D.C. Singleton, C.M. Rogers, O.P. Monteiro, J.M. Bennett, R. Baronio, S. Muller, D.L. Daniels, J. Mendez, S. Knapp, P.E. Brennan, D.J. Dixon, LP99: discovery and synthesis of the first selective BRD7/9 bromodomain inhibitor, *Angew. Chem. Int. Ed. Engl.* 54 (2015) 6217–6221.
- [13] L.J. Martin, M. Koegl, G. Bader, X.L. Cockcroft, O. Fedorov, D. Fiegen, T. Gerstberger, M.H. Hofmann, A.F. Hohmann, D. Kessler, S. Knapp, P. Knesl, S. Kornigg, S. Muller, H. Nar, C. Rogers, K. Rumpel, O. Schaaf, S. Steurer, C. Tallant, C.R. Vakoc, M. Zeeb, A. Zoepfel, M. Pearson, G. Boehmelt, D. McConnell, Structure-based design of an in vivo active selective BRD9 inhibitor, *J. Med. Chem.* 59 (2016) 4462–4475.
- [14] N.H. Theodoulou, P. Bamorough, A.J. Bannister, I. Becher, R.A. Bit, K.H. Che, C.W. Chung, A. Dittmann, G. Drewes, D.H. Drewry, L. Gordon, P. Grandi, M. Leveridge, M. Lindon, A.M. Michon, J. Molnar, S.C. Robson, N.C. Tomkinson, T. Kouzarides, R.K. Prinjha, P.G. Humphreys, Discovery of I-BRD9, a selective cell active chemical probe for bromodomain containing protein 9 inhibition, *J. Med. Chem.* 59 (2016) 1425–1439.
- [15] P. Chen, A. Chaikuad, P. Bamorough, M. Bantscheff, C. Bountra, C.W. Chung, O. Fedorov, P. Grandi, D. Jung, R. Lesniak, M. Lindon, S. Muller, M. Philpott, R. Prinjha, C. Rogers, C. Selenski, C. Tallant, T. Werner, T.M. Willson, S. Knapp, D.H. Drewry, Discovery and characterization of GSK2801, a selective chemical probe for the bromodomains BAZ2A and BAZ2B, *J. Med. Chem.* 59 (2016) 1410–1424.
- [16] L. Drouin, S. McGrath, L.R. Vidler, A. Chaikuad, O. Monteiro, C. Tallant, M. Philpott, C. Rogers, O. Fedorov, M. Liu, W. Akhtar, A. Hayes, F. Raynaud, S. Muller, S. Knapp, S. Hoelder, Structure enabled design of BAZ2-ICR, a chemical probe targeting the bromodomains of BAZ2A and BAZ2B, *J. Med. Chem.* 58 (2015) 2553–2559.
- [17] B.S. Gerstenberger, J.D. Trzupke, C. Tallant, O. Fedorov, P. Filippakopoulos, P.E. Brennan, V. Fedele, S. Martin, S. Picaud, C. Rogers, M. Parikh, A. Taylor, B. Samas, A. O'Mahony, E. Berg, G. Pallares, A.D. Torrey, D.K. Treiber, I.J. Samardjiev, B.T. Nasipak, T. Padilla-Benavides, Q. Wu, A.N. Imbalzano, J.A. Nickerson, M.E. Bunnage, S. Muller, S. Knapp, D.R. Owen, Identification of a chemical probe for family VIII bromodomains through optimization of a fragment hit, *J. Med. Chem.* 59 (2016) 4800–4811.
- [18] M. Moustakim, P.G. Clark, L. Trullii, A.L. Fuentes de Arriba, M.T. Ehebauer, A. Chaikuad, E.J. Murphy, J. Mendez-Johnson, D. Daniels, C.D. Hou, Y.H. Lin, J.R. Walker, R. Hui, H. Yang, L. Dorrell, C.M. Rogers, O.P. Monteiro, O. Fedorov, K.V. Huber, S. Knapp, J. Heer, D.J. Dixon, P.E. Brennan, Discovery of a PCAF bromodomain chemical probe, *Angew. Chem. Int. Ed. Engl.* 56 (2017) 827–831.
- [19] P. Bamorough, C.W. Chung, E.H. Demont, R.C. Furze, A.J. Bannister, K.H. Che, H. Diallo, C. Douault, P. Grandi, T. Kouzarides, A.M. Michon, D.J. Mitchell, R.K. Prinjha, C. Rau, S. Robson, R.J. Sheppard, R. Upton, R.J. Watson, A chemical probe for the ATAD2 bromodomain, *Angew. Chem. Int. Ed. Engl.* 55 (2016) 11382–11386.
- [20] A. Vezzoli, N. Bonadies, M.D. Allen, S.M. Freund, C.M. Santiveri, B.T. Kvinlaug, B.J. Huntly, B. Gottgens, M. Bycroft, Molecular basis of histone H3K36me3 recognition by the PWWP domain of Brpf1, *Nat. Struct. Mol. Biol.* 17 (2010) 617–619.
- [21] A. Poplawski, K. Hu, W. Lee, S. Natesan, D. Peng, S. Carlson, X. Shi, S. Balaz, J.L. Markley, K.C. Glass, Molecular insights into the recognition of N-terminal histone modifications by the BRPF1 bromodomain, *J. Mol. Biol.* 426 (2014) 1661–1676.
- [22] T. Brown, J. Swansbury, M.M. Taj, Prognosis of patients with t(8;16)(p11;p13)

- acute myeloid leukemia, *Leuk. Lymphoma* 53 (2012) 338–341.
- [23] J. Borrow, V.P. Stanton Jr., J.M. Andresen, R. Becher, F.G. Behm, R.S. Chaganti, C.I. Civin, C. Disteché, I. Dube, A.M. Frischauf, D. Horsman, F. Mitelman, S. Volinia, A.E. Watmore, D.E. Housman, The translocation t(8;16)(p11;p13) of acute myeloid leukaemia fuses a putative acetyltransferase to the CREB-binding protein, *Nat. Genet.* 14 (1996) 33–41.
- [24] I. Kitabayashi, Y. Aikawa, A. Yokoyama, F. Hosoda, M. Nagai, N. Kakazu, T. Abe, M. Ohki, Fusion of MOZ and p300 histone acetyltransferases in acute monocytic leukemia with a t(8;22)(p11;q13) chromosome translocation, *Leukemia* 15 (2001) 89–94.
- [25] M. Carapeti, R.C. Aguiar, J.M. Goldman, N.C. Cross, A novel fusion between MOZ and the nuclear receptor coactivator TIF2 in acute myeloid leukemia, *Blood* 91 (1998) 3127–3133.
- [26] P.J. Troke, K.B. Kindle, H.M. Collins, D.M. Heery, MOZ fusion proteins in acute myeloid leukaemia, *Biochem. Soc. Symp.* (2006) 23–39.
- [27] P. Bamborough, H.A. Barnett, I. Becher, M.J. Bird, C.W. Chung, P.D. Craggs, E.H. Demont, H. Diallo, D.J. Fallon, L.J. Gordon, P. Grandi, C.I. Hobbs, E. Hooper-Greenhill, E.J. Jones, R.P. Law, A. Le Gall, D. Lugo, A.M. Michon, D.J. Mitchell, R.K. Prinjha, R.J. Sheppard, A.J. Watson, R.J. Watson, GSK6853, a chemical probe for inhibition of the BRPF1 bromodomain, *ACS Med. Chem. Lett.* 7 (2016) 552–557.
- [28] J. Bennett, O. Fedorov, C. Tallant, O. Monteiro, J. Meier, V. Gamble, P. Savitsky, G.A. Nunez-Alonso, B. Haendler, C. Rogers, P.E. Brennan, S. Muller, S. Knapp, Discovery of a chemical tool inhibitor targeting the bromodomains of TRIM24 and BRPF, *J. Med. Chem.* 59 (2016) 1642–1647.
- [29] N. Igoe, E.D. Bayle, O. Fedorov, C. Tallant, P. Savitsky, C. Rogers, D.R. Owen, G. Deb, T.C. Somerville, D.M. Andrews, N. Jones, A. Cheasty, H. Ryder, P.E. Brennan, S. Muller, S. Knapp, P.V. Fish, Design of a biased potent small molecule inhibitor of the bromodomain and PHD finger-containing (BRPF) proteins suitable for cellular and in vivo studies, *J. Med. Chem.* 60 (2017) 668–680.
- [30] N. Igoe, E.D. Bayle, C. Tallant, O. Fedorov, J.C. Meier, P. Savitsky, C. Rogers, Y. Morias, S. Scholze, H. Boyd, D. Cunoosamy, D.M. Andrews, A. Cheasty, P.E. Brennan, S. Muller, S. Knapp, P.V. Fish, Design of a chemical probe for the bromodomain and plant homeodomain finger-containing (BRPF) family of proteins, *J. Med. Chem.* 60 (2017) 6998–7011.
- [31] J. Zhu, A. Caflich, Twenty crystal structures of bromodomain and PHD finger containing protein 1 (BRPF1)/Ligand complexes reveal conserved binding motifs and rare interactions, *J. Med. Chem.* 59 (2016) 5555–5561.
- [32] P. Sledz, A. Caflich, Protein structure-based drug design: from docking to molecular dynamics, *Curr. Opin. Struct. Biol.* 48 (2017) 93–102.
- [33] H. Zhao, A. Caflich, Molecular dynamics in drug design, *Eur. J. Med. Chem.* 91 (2015) 4–14.
- [34] D.R. Koes, C.J. Camacho, ZINCPharmer: pharmacophore search of the ZINC database, *Nucleic Acids Res.* 40 (2012) W409–W414.
- [35] O. Trott, A.J. Olson, AutoDock Vina: improving the speed and accuracy of docking with a new scoring function, efficient optimization, and multi-threading, *J. Comput. Chem.* 31 (2010) 455–461.
- [36] L.W. Elizabeth Quinn, Pietro Ciceri, Gabriel Pallares, Elyssa Pickle, Adam Torrey, Mark Floyd, Jeremy Hunt, Daniel Treiber, BROMOscan - a high throughput, quantitative ligand binding platform identifies best-in-class bromodomain inhibitors from a screen of mature compounds targeting other protein classes, *Canc. Res.* 2013 (2013) 4238.
- [37] J.J. Irwin, T. Sterling, M.M. Mysinger, E.S. Bolstad, R.G. Coleman, ZINC: a free tool to discover chemistry for biology, *J. Chem. Inf. Model.* 52 (2012) 1757–1768.
- [38] B.R. Brooks, C.L. Brooks 3rd, A.D. Mackerell Jr., L. Nilsson, R.J. Petrella, B. Roux, Y. Won, G. Archontis, C. Bartels, S. Boresch, A. Caflich, L. Caves, Q. Cui, A.R. Dinner, M. Feig, S. Fischer, J. Gao, M. Hodoscek, W. Im, K. Kuczera, T. Lazaridis, J. Ma, V. Ovchinnikov, E. Paci, R.W. Pastor, C.B. Post, J.Z. Pu, M. Schaefer, B. Tidor, R.M. Venable, H.L. Woodcock, X. Wu, W. Yang, D.M. York, M. Karplus, CHARMM: the biomolecular simulation program, *J. Comput. Chem.* 30 (2009) 1545–1614.
- [39] J.R. Marchand, A. Dalle Vedove, G. Lolli, A. Caflich, Discovery of inhibitors of four bromodomains by fragment-anchored ligand docking, *J. Chem. Inf. Model.* 57 (2017) 2584–2597.
- [40] G. Neudert, G. Klebe, DSX: a knowledge-based scoring function for the assessment of protein-ligand complexes, *J. Chem. Inf. Model.* 51 (2011) 2731–2745.
- [41] M. Philpott, J. Yang, T. Tumber, O. Fedorov, S. Uttarkar, P. Filippakopoulos, S. Picaud, T. Keates, I. Felletar, A. Ciulli, S. Knapp, T.D. Heightman, Bromodomain-peptide displacement assays for interactome mapping and inhibitor discovery, *Mol. Biosyst.* 7 (2011) 2899–2908.
- [42] A. Magno, S. Steiner, A. Caflich, Mechanism and kinetics of acetyl-lysine binding to bromodomains, *J. Chem. Theor. Comput.* 9 (2013) 4225–4232.
- [43] S. Steiner, A. Magno, D. Huang, A. Caflich, Does bromodomain flexibility influence histone recognition? *FEBS Lett.* 587 (2013) 2158–2163.
- [44] D.S. Hewings, M. Wang, M. Philpott, O. Fedorov, S. Uttarkar, P. Filippakopoulos, S. Picaud, C. Vuppasetty, B. Marsden, S. Knapp, S.J. Conway, T.D. Heightman, 3,5-dimethylisoxazoles act as acetyl-lysine-mimetic bromodomain ligands, *J. Med. Chem.* 54 (2011) 6761–6770.
- [45] D.S. Hewings, O. Fedorov, P. Filippakopoulos, S. Martin, S. Picaud, A. Tumber, C. Wells, M.M. Olcina, K. Freeman, A. Gill, A.J. Ritchie, D.W. Sheppard, A.J. Russell, E.M. Hammond, S. Knapp, P.E. Brennan, S.J. Conway, Optimization of 3,5-dimethylisoxazole derivatives as potent bromodomain ligands, *J. Med. Chem.* 56 (2013) 3217–3227.
- [46] O. Mirguet, Y. Lamotte, F. Donche, J. Toum, F. Gellibert, A. Bouillot, R. Gosmini, V.L. Nguyen, D. Delannee, J. Seal, F. Blandel, A.B. Boullay, E. Boursier, S. Martin, J.M. Brusq, G. Krysa, A. Riou, R. Tellier, A. Costaz, P. Huet, Y. Dudit, L. Trotter, J. Kirilovsky, E. Nicodeme, From ApoA1 upregulation to BET family bromodomain inhibition: discovery of I-BET151, *Bioorg. Med. Chem. Lett.* 22 (2012) 2963–2967.
- [47] J. Seal, Y. Lamotte, F. Donche, A. Bouillot, O. Mirguet, F. Gellibert, E. Nicodeme, G. Krysa, J. Kirilovsky, S. Beinke, S. McCleary, I. Rioja, P. Bamborough, C.W. Chung, L. Gordon, T. Lewis, A.L. Walker, L. Cutler, D. Lugo, D.M. Wilson, J. Witherington, K. Lee, R.K. Prinjha, Identification of a novel series of BET family bromodomain inhibitors: binding mode and profile of I-BET151 (GSK1210151A), *Bioorg. Med. Chem. Lett.* 22 (2012) 2968–2972.
- [48] G. Klebe, Applying thermodynamic profiling in lead finding and optimization, *Nat. Rev. Drug Discov.* 14 (2015) 95–110.
- [49] M. Xu, A. Unzue, J. Dong, D. Spiliotopoulos, C. Nevado, A. Caflich, Discovery of CREBBP bromodomain inhibitors by high-throughput docking and hit optimization guided by molecular dynamics, *J. Med. Chem.* 59 (2016) 1340–1349.
- [50] A. Unzue, H. Zhao, G. Lolli, J. Dong, J. Zhu, M. Zechner, A. Dolbois, A. Caflich, C. Nevado, The “gatekeeper” residue influences the mode of binding of acetyl indoles to bromodomains, *J. Med. Chem.* 59 (2016) 3087–3097.
- [51] K. Vanommeslaeghe, A.D. MacKerell Jr., Automation of the CHARMM General Force Field (CGenFF) I: bond perception and atom typing, *J. Chem. Inf. Model.* 52 (2012) 3144–3154.
- [52] G. Landrum, RDKit: open-source cheminformatics, in.
- [53] S. Keller, C. Vargas, H. Zhao, G. Piszczek, C.A. Brautigam, P. Schuck, High-precision isothermal titration calorimetry with automated peak-shape analysis, *Anal. Chem.* 84 (2012) 5066–5073.
- [54] H. Zhao, G. Piszczek, P. Schuck, SEDPHAT—a platform for global ITC analysis and global multi-method analysis of molecular interactions, *Methods* 76 (2015) 137–148.
- [55] C.A. Brautigam, H. Zhao, C. Vargas, S. Keller, P. Schuck, Integration and global analysis of isothermal titration calorimetry data for studying macromolecular interactions, *Nat. Protoc.* 11 (2016) 882–894.
- [56] W. Kabsch, Integration, scaling, space-group assignment and post-refinement, *Acta Crystallogr D Biol Crystallogr* 66 (2010) 133–144.
- [57] P.R. Evans, G.N. Murshudov, How good are my data and what is the resolution? *Acta Crystallogr D Biol Crystallogr* 69 (2013) 1204–1214.
- [58] A. Vagin, A. Teplyakov, Molecular replacement with MOLREP, *Acta Crystallogr D Biol Crystallogr* 66 (2010) 22–25.
- [59] M.D. Winn, C.C. Ballard, K.D. Cowtan, E.J. Dodson, P. Emsley, P.R. Evans, R.M. Keegan, E.B. Krissinel, A.G. Leslie, A. McCoy, S.J. McNicholas, G.N. Murshudov, N.S. Pannu, E.A. Potterton, H.R. Powell, R.J. Read, A. Vagin, K.S. Wilson, Overview of the CCP4 suite and current developments, *Acta Crystallogr D Biol Crystallogr* 67 (2011) 235–242.
- [60] P.D. Adams, P.V. Afonine, G. Bunkoczi, V.B. Chen, I.W. Davis, N. Echols, J.J. Headd, L.W. Hung, G.J. Kapral, R.W. Grosse-Kunstleve, A.J. McCoy, N.W. Moriarty, R. Oeffner, R.J. Read, D.C. Richardson, J.S. Richardson, T.C. Terwilliger, P.H. Zwart, PHENIX: a comprehensive Python-based system for macromolecular structure solution, *Acta Crystallogr D Biol Crystallogr* 66 (2010) 213–221.
- [61] P. Emsley, B. Lohkamp, W.G. Scott, K. Cowtan, Features and development of coot, *Acta Crystallogr D Biol Crystallogr* 66 (2010) 486–501.
- [62] A.W. Schuttelkopf, D.M. van Aalten, PRODRG: a tool for high-throughput crystallography of protein-ligand complexes, *Acta Crystallogr D Biol Crystallogr* 60 (2004) 1355–1363.
- [63] S. Pronk, S. Pall, R. Schulz, P. Larsson, P. Bjelkmar, R. Apostolov, M.R. Shirts, J.C. Smith, P.M. Kasson, D. van der Spoel, B. Hess, E. Lindahl, GROMACS 4.5: a high-throughput and highly parallel open source molecular simulation toolkit, *Bioinformatics* 29 (2013) 845–854.
- [64] D. Spiliotopoulos, E.C. Wamhoff, G. Lolli, C. Rademacher, A. Caflich, Discovery of BAZ2A bromodomain ligands, *Eur. J. Med. Chem.* 139 (2017) 564–572.
- [65] D. Spiliotopoulos, J. Zhu, E.C. Wamhoff, N. Deearin, J.R. Marchand, J. Aretz, C. Rademacher, A. Caflich, Virtual screen to NMR (VS2NMR): discovery of fragment hits for the CBP bromodomain, *Bioorg. Med. Chem. Lett.* 27 (2017) 2472–2478.
- [66] J. Huang, A.D. MacKerell Jr., CHARMM36 all-atom additive protein force field: validation based on comparison to NMR data, *J. Comput. Chem.* 34 (2013) 2135–2145.